CODANIN-1 sequesters ASF1 by using a histone H3 mimic helix to regulate histone supply

Tae-Kyeong Jeong[1,*], R. Ciaran MacKenzie Frater[2,*], Anja Groth[2,3,4,#], Ji-Joon Song[1,#]

[1]Department of Biological Sciences, KI for the BioCentury, Korea Advanced Institute of Science and Technology (KAIST), Daejeon 34141, Korea.

[2]The Novo Nordisk Foundation Center for Protein Research (CPR), University of Copenhagen, Copenhagen, Denmark.

[3]Biotech Research & Innovation Centre, University of Copenhagen, Copenhagen 2200, Denmark.

[4]Department of Cellular and Molecular Medicine, University of Copenhagen, Copenhagen 2200, Denmark.

*These authors contributed equally

[#] Correspondence should be addressed to anja.groth@cpr.ku.dk (A.G.), songj@kaist.ac.kr (J.S.)

Abstract

ASF1 is a major histone chaperone that regulates the supply of histone H3-H4 and facilitates nucleosome assembly, essential for maintaining chromatin structure. CODANIN-1 negatively regulates the function of ASF1. However, the molecular mechanism by which CODANIN-1 inhibits ASF1-mediated histone supply remains elusive. Here, we present the cryo-electron microscopy (cryo-EM) structure of a human CODANIN-1_ASF1A_CDIN1 complex at 3.56 Å resolution. The structure reveals that CODANIN-1 forms a dimer and utilizes a histone H3 mimic helix (HMH) to interact with the histone binding surface of ASF1. This feature confers on CODANIN-1 an ability to sequester ASF1 and inhibit the formation of the ASF1-H3-H4 complex, essential for histone nuclear import and nucleosome assembly. Furthermore, we show that interaction of both the CODANIN-1 HMH and B-domain with ASF1 is critical for the inhibitory activity of CODANIN-1 in cells. Our study provides a structural and molecular basis for the function of CODANIN-1 as a unique negative regulator of nucleosome assembly.

Introduction

Eukaryotic DNA is organized into a dynamic multilayered structure called chromatin. Regulating the organization and structure of chromatin is essential to maintain and express genomic information. The fundamental repeating unit of chromatin is the nucleosome, consisting of two copies of each of the four core histones (H3, H4, H2A and H2B) and 147 base pairs of DNA[1]. The nucleosome is a dynamic structure and the major target of chromatin regulation. Nucleosome position and structure are remodeled in an ATP-dependent manner and the histones are covalently modified with various moieties including methyl, acetyl, phosphoryl, and ubiquitin[2-4]. The combination of nucleosome remodeling and histone modifications governs genome regulation. Nucleosomes are dynamically assembled and disassembled during cellular processes such as DNA replication and transcription[5-7]. The assembly of nucleosome occurs in a step-wise manner, which is assisted and regulated by a group of protein factors called histone chaperones, which interact with histones and facilitate their delivery to chromatin and assembly into nucleosomes. Anti-silencing function 1 (ASF1) is a major histone chaperone for histone H3-H4 in both the cytoplasm and the nucleus[5,8]. In mammals, two ASF1 isoforms (ASF1A and ASF1B) exist and they show the high level of sequence conservation except the C-terminal unstructured region. While ASF1A is ubiquitously expressed in cells, ASF1B is mainly expressed in proliferating cells[9]. In the cytoplasm, newly synthesized histone H3-H4 dimers are formed by DNAJC9 and NASP before they are modified by the HAT1_RbAP48/46 histone acetyltransferase complex at lysine 5 and 12 on histone H4[10-14]. ASF1 in turn directly interacts with histone H3-H4 in complex with NASP and mediates the nuclear import of histone H3-H4 by importins[10,11,15,16]. In the nucleus, ASF1 delivers histone H3-H4 dimers to CAF-1[17,18] and the HIRA[19-21] complexes for nucleosome assembly during replication dependent and independent processes respectively. Thus, ASF1 directly regulates the flow of newly synthesized histone H3-H4 to chromatin across the cell cycle, with its major task to supply histones for DNA replication in S-phase [8,22-24]. ASF1 directly interacts with αH3 helix of histone H3, a part of the histone H3-H4 tetramerization interface and prevents histone H3-H4 forming a tetramer before nucleosome assembly[25,26]. To handover histones, ASF1 interacts with the B-domains in CAF-1 and HIRA using an interface on its opposite side to its histone binding surface[27,28]. We previously identified that CODANIN-1 interacts with ASF1 via a B-domain and negatively regulates the function of ASF1[29]. Overexpression of CODANIN-1 sequesters ASF1 in the cytoplasm and induces cell cycle arrest in S-phase, suggesting that CODANIN-1 inhibits ASF1-mediated histone supply. CODANIN-1 encoded by *CDAN1* forms a complex with CDAN1 interacting Nuclease 1 (CDIN1)[30-32]. Like ASF1A, CODANIN-1 and CDIN1 are ubiquitously expressed, and mutations in CDAN1 or CDIN1 can cause the rare, autosomal recessive disease, Congenital Dyserythropoietic Anemia type I (CDA-I)[33,34]. CDA-I is characterized by defective terminal erythropoiesis and nuclear abnormalities such as a spongy appearance of heterochromatin in erythroblasts [35-37]. While the exact function of CODANIN-1

and CDIN1 in erythropoiesis is unknown, its interaction with ASF1 suggests a role in regulation of histone dynamics that might become critical for chromatin compaction in late stages of erythropoiesis. In this study, we provide structural and molecular basis on the mechanism by which CODANIN-1 sequesters and inactivates ASF1.

Results

Cryo-EM Structure of the CODANIN-1 complex

To investigate the molecular mechanism of the interplay between CODANIN-1 and ASF1, we determined the cryo-EM structure of CODANIN-1 complex composed of full-length CODANIN-1 (1-1,227 a.a.), ASF1A (1-172 a.a.) and full-length CDIN1 (a.k.a. C15ORF141) (1-281 a.a.) (Fig. 1a). The CODANIN-1 complex exhibits 400 kDa in its size estimated by a size-exclusion chromatography (Fig. 1b), suggesting that CODANIN-1 form a multimer. For cryo-EM study, we further purified CODANIN-1 complex with GraFix and collected 4,282 micrographs using a Titan Krios with Gatan K3 detector. We then processed the data generating 3.56 Å resolution structure of the CODANIN-1 complex (Fig. 1c,d, Extended Data Fig. 1a-c and Table 1). The high quality of the cryo-EM map enabled us to generate an atomic model of the CODANIN-1 complex (Fig. 1f and Extended Data Fig. 2). The C-terminal region of CODANIN-1 and the entire CDIN1 were not visible in the cryo-EM map. As CDIN1 is known to tethers to the flexible C-terminal domain of CODANIN-1, the CDIN1 together with the CODANIN-1 C-terminal region are likely very flexible[30-32]. The cryo-EM structure shows that CODANIN-1 dimerizes with each monomer binding one ASF1A molecule, forming a heterotetrametric complex with a 2-fold rotational symmetry (Fig. 1e,f). This configuration is consistent with the estimated size of the complex by size-exclusion chromatography (Fig. 1b). CODANIN-1 entirely consists of α-helices (Fig. 1f and Extended Data Figs. 3 and 4). The helices are linked by disordered loops. Specifically, most of a large loop (69-284 a.a.) linking αH4 and αH5 is completely disordered in the cryo-EM map. In addition, the region beyond 818 a.a. is not visible in the cryo-EM structure despite that the C-terminal region is predicted to be composed of α-helices. CODANIN-1 is composed of two lobes: α-helices from αH1 to αH12 along with αH29 form one lobe (LOBE1) and helices from αH13 to αH28 (except αH16) forms the other lobe (LOBE2) (Fig.1e and Extended Data Fig. 4). Interestingly, αH16 is located between the two lobes and interacts with ASF1A. LOBE2 from the two CODANIN-1 molecules make extensive interactions with each other to form a dimer with a dimerization area of 1,844 $Å^2$ for the each CODANIN-1. This large dimerization interface implies that CODANIN-1 forms an obligatory dimer. Overall, the cryo-EM structure of CODANIN-1 complex delineates the structural features of CODANIN-1_ASF1A complex.

Figure 1

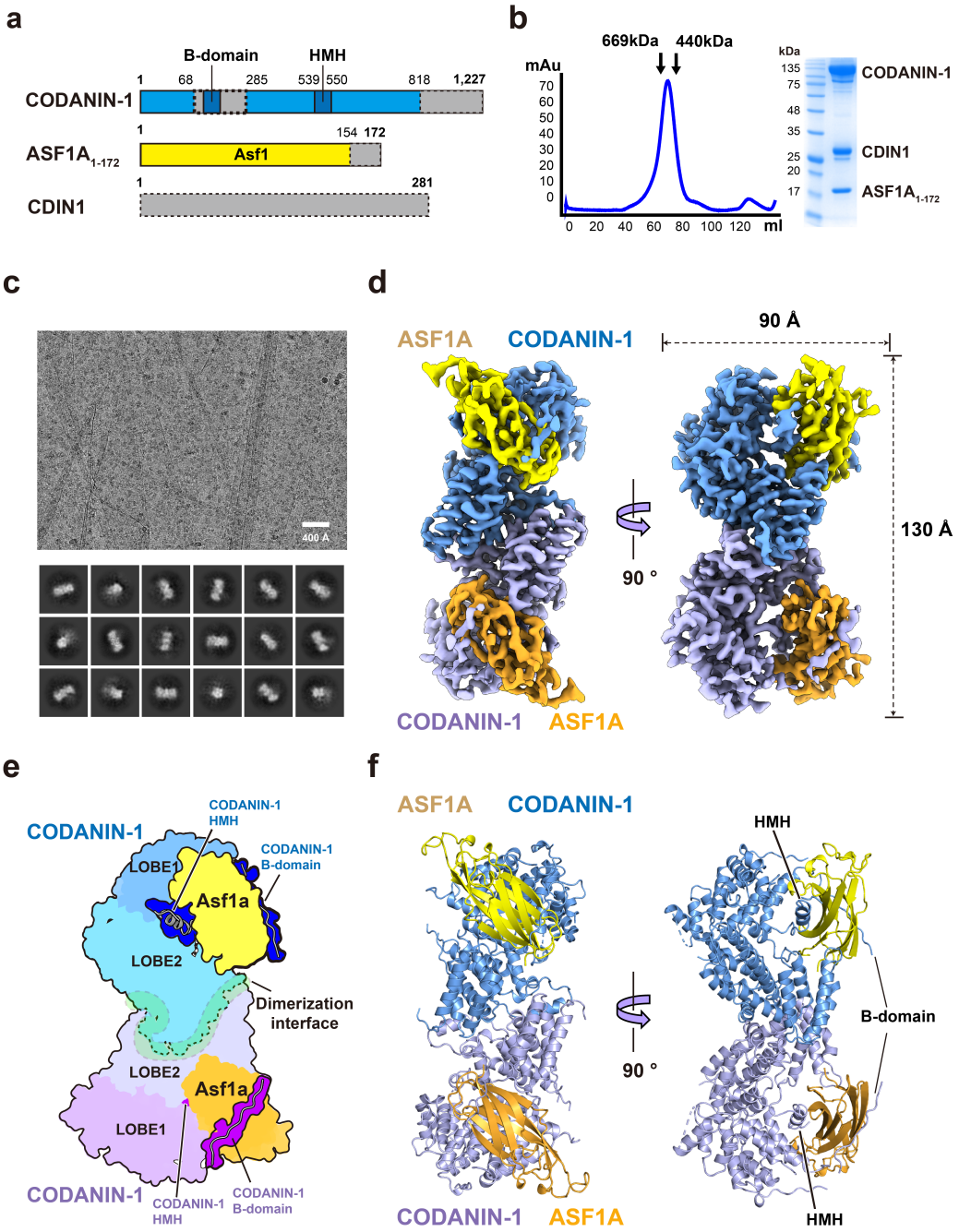

Fig. 1 Cryo-EM structure of CODANIN-1 complex.
a, A schematic diagram of CODANIN-1 complex composed of CODANIN-1 full-length (1-1,227), C-terminal truncated ASF1A$_{1-172}$ (1-172 a.a.) and CDIN1 (1-281 a.a.). Dotted gray boxes indicate the disordered region in the cryo-EM map. **b**, A gel filtration profile and an SDS PAGE gel of CODANIN-1 complex. **c**, A representative cryo-EM micrograph of CODANIN-1 complex on a graphene oxide covered grid and 2D Class-averages. **d**, The cryo-EM map of CODANIN-1 complex. Two CODANIN-1 molecules in a dimer are colored in pale blue and pale purple and the bound ASF1A in yellow and orange. **e,** A schematic diagram of the structure of CODANIN-1 complex. **f**, An atomic structure of CODANIN-1 complex is shown in a ribbon diagram.

CODANIN-1 utilizes a histone mimic helix (HMH) to interact with ASF1A.

Our cryo-EM structure delineates the ASF1 binding mode of CODANIN-1. ASF1A is wrapped by the several regions of CODANIN-1, including the previously identified B-domain[29], αH29 helix, a loop linking αH13 and αH14 helices, and the αH16 helix. Thus, CODANIN-1 basically encapsulates ASF1A (Fig. 2a). The B-domain (193-203 a.a.) is located in the middle of a large loop (69-284 a.a.), which is completely disordered except the B-domain tethered to ASF1A. Therefore, this loop including the B-domain is likely disordered when CODANIN-1 is not bound to ASF1A. The B-domain of CODANIN-1 interacts with ASF1A in a similar manner as other B-domain proteins (Extended Data Fig. 5a). Arg195 and Arg196 of CODANIN-1 make salt bridges with Asp58 and Asp37 respectively (Fig. 2b). These salt bridges are also found in other B-domain-ASF1 interactions such as HIRA[27] and CAF-1[28] (Extended Data Fig. 5a).

Interestingly, αH16 helix (539-550 a.a.) interacts with the histone binding pocket of ASF1A, suggesting that the ASF1A binding to CODANIN-1 and histone H3-H4 is mutually exclusive (Fig. 2c). Moreover, the amino acid sequence of αH16 helix is very similar to that of αH3 helix of histone H3, as if this αH16 helix mimics the αH3 helix of histone H3 that binds to ASF1A [25,26] (Fig.2c). Therefore, we designated the αH16 helix as the 'Histone Mimic Helix (HMH)'. The detailed interaction between HMH and ASF1A is also very similar to that of histone H3 and ASF1A. Specifically, Leu545 and Leu549 of the HMH from hydrophobic interactions with Val94 and Leu96 of ASF1A. ASF1A Val94 is shown to be critical for the interaction with histone H3[25,26]. In addition, Arg541 and Arg548 of the HMH make salt bridges with Asp88 and Asp54 of ASF1A (Fig.2c). Therefore, CODANIN-1 seems to harness the binding mode of ASF1A and histone H3 to sequester ASF1A with its HMH. These data immediately explain why a mutation in the ASF1A histone binding sites (V94R) disrupted association with CODANIN-1 in a recent proteomics study of the histone chaperone network[38].

Figure 2

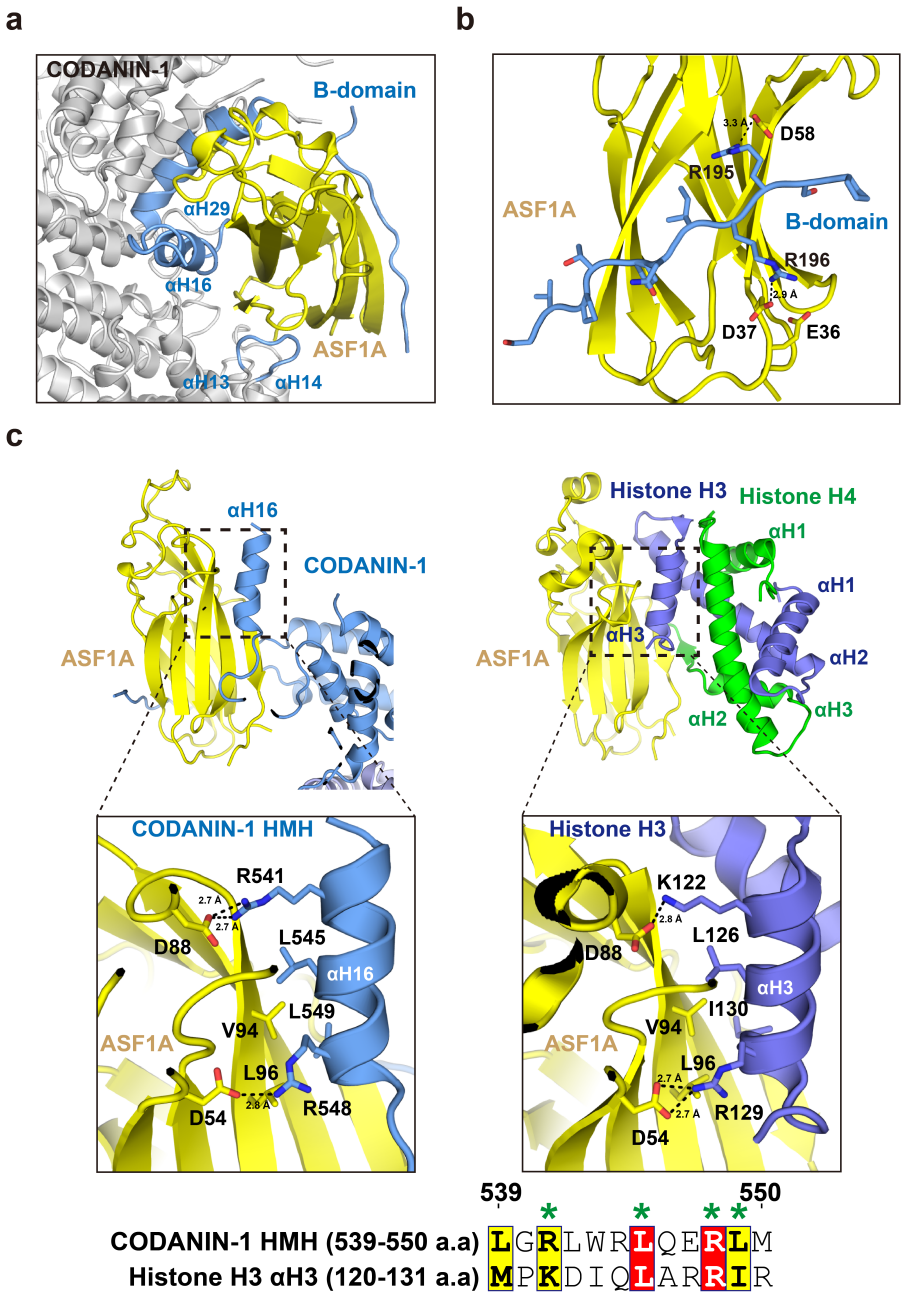

Fig. 2 CODANIN-1 interacts with ASF1A using B-domain and Histone Mimic Helix (HMH). **a,** CODANIN-1 encapsulates ASF1A using the B-domain, αH29 helix, a loop linking αH13 and αH14 helices, and αH16 helix. **b**, Detailed interactions between ASF1A and the B-domain (193-203 a.a.) of CODANIN-1. D37 and D58 in ASF1A form salt bridges with R196 and R195 in the B-domain respectively. **c**, A comparison of the interaction mode of Histone Mimic Helix (HMH) of CODANIN-1 with ASF1A (left panel) with that of histone H3-H4 and ASF1A complex (PDB 2IO5, right panel). The HMH (αH16 helix) occupies the histone H3 αH3-binding pockets of ASF1A (left panel). V94 of ASF1A forms hydrophobic interaction with L545 and L549 in HMH. D88 and D54 in ASF1A form salt bridges with R541 and R548 in HMH. A sequence comparison between CODANIN-1 HMH and histone H3 αH3 (bottom panel). The residues interacting with ASF1A are marked with green asterisks.

The HMH and B-domain of CODANIN-1 participate in ASF1A binding

The cryo-EM structure shows that CODANIN-1 utilizes both the HMH and the B-domain to interact with ASF1A. We first asked whether each HMH or B-domain is sufficient for binding with ASF1A. We generated GST-HMH (520-557 a.a.) and GST-B-domain (183-217 a.a.) and performed GST pulldown assays for ASF1A binding (Fig. 3a). The pulldown assay showed that each domain is sufficient for ASF1A binding, suggesting that the HMH and B-domain domain may function independently. To examine the interaction mode between CODANIN-1 and ASF1A based on the cryo-EM structure, we generated R541A and R548A mutants in GST-HMH, which would disrupt the salt bridge interaction with D88 and D54 residues in ASF1A. In addition, we made a L545A/L549A (LL/AA) double mutant to eliminate hydrophobic interactions between the CODANIN-1 HMH and ASF1. GST-pulldown assay with these HMH mutants showed these mutations abrogate the interaction with ASF1A, further validating that CODANIN-1 uses a histone-mimicking mechanism to interact with ASF1 (Fig. 3a). For the B-domain, we introduced R195A/R196A mutation (B_{mut}) in GST-B-domain, which would disrupt the two salt bridge interactions observed in our structure. We then performed GST pulldown experiments, showing that this B-domain mutant lost the interaction with ASF1A (Fig. 3a). These results reveal that CODANIN-1 utilizes both the HMH and the B-domain to interact with ASF1A.

To examine the contribution of HMH and B-domain to ASF1 binding in the context of full-length CODANIN-1, we conducted GST-pulldown experiments with full-length wildtype (WT) and mutant CODANIN-1 proteins using GST-ASF1A as a bait (Fig. 3b). First, to examine the contribution of the HMH toward ASF1 binding, we mutated Arg541 or Arg548 in the HMH to alanines (R541A, R548A) predicted to disrupt the salt bridges with ASF1A Asp88 or Asp54, respectively (Fig. 2c). We also attempted to disrupt the hydrophobic interaction between the HMH and ASF1A by mutating both Leu545 and Leu549 to alanines (LL/AA: L545A/L549A) (Fig. 2c). Second, we generated an R195A/R196A mutant in the B-domain (B_{mut}: R195A/R196A). We then performed GST-pulldown assay with these mutants (Fig. 3b). Unexpectedly, all mutants bound ASF1A comparable to wildtype CODANIN-1. This suggests that the HMH and B-domain independently contribute to ASF1A binding with each domain being sufficient. Therefore, we generated double mutants (R541A+B_{mut}, R548A+B_{mut}, LL/AA+B_{mut}) where both the HMH (R541, R548, or L545/L549) and B-domain (R195 and R196) were mutated and examined their binding to ASF1A. While the R541A+B_{mut} mutant displayed a modest reduction in ASF1a binding, the R548A+B_{mut} and LL/AA+B_{mut} abrogated CODANIN-1 binding to ASF1A (Fig. 3b). Furthermore, we quantitatively analyzed the effect of the HMH and B domain mutations using Bio-Layer Interferometry (BLI) (Extended Data Fig. 6). We used ASF1A as a ligand and CODANIN-1 wildtype, HMH mutant (LL/AA: L545A/L549A), B-domain mutant (B_{mut}: R195A/R196A) and a double mutant (LL/AA+B_{mut}) as analytes. BLI analysis shows that wild type CODANIN-1 has picomolar apparent binding affinity toward ASF1. Consistent

with the GST-pulldown experiments, CODANIN-1 HMH mutant (LL/AA) shows comparable binding to the wild type, while the B-domain mutation (B_{mut}) moderately impaired the interaction but still showed nanomolar apparent binding affinity. However, when both HMH and B-domain was mutated (LL/AA+B_{mut}), the binding of CODANIN-1 to ASF1 was completely abrogated, which is also consistent with the GST pulldown experiments. Next, we designed complementary mutants in ASF1A to disrupt the interaction with CODANIN-1 HMH and B-domain and performed GST-pulldown assay using each ASF1A mutant as a bait and full-length CODANIN-1 as a prey. We introduced mutations at the ASF1A HMH binding surface (D88A, D54A, or V94R) and the B-domain binding site (ED/AA: E36A/D37A) as well as a double mutant (Fig. 3c). Consistent with the mutational analysis of CODANIN-1, single ASF1A mutations in the HMH or B-domain interactions sites had modest effect on the binding, while the double mutant significantly abrogates ASF1A binding to CODANIN-1 (Fig. 3c). Together with our cryo-EM structure, these data argue that the HMH and B-domain are the major ASF1A binding motifs in CODANIN-1 and that they function independently for ASF1A binding.

Figure 3

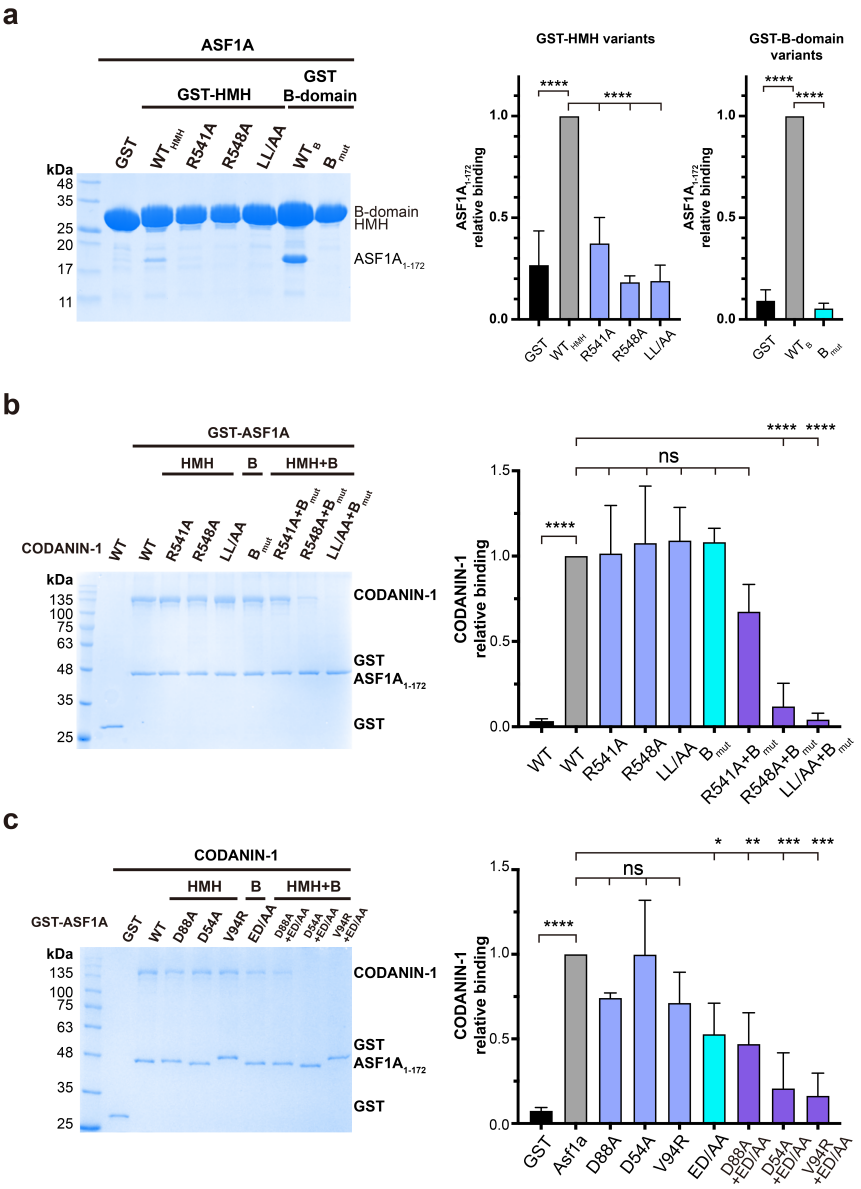

Fig. 3 HMH and B-domain of CODANIN-1 independently contribute to ASF1 binding.
a, GST-pulldown experiments with GST-HMH (520-557 a.a.) and GST-B-domain (183-217 a.a.) or their mutants for ASF1A binding (HMH mutants: R541A, R548A or LL/AA; B domain mutant: B_{mut}-R195A/R196A). **b,** GST-pulldown experiments with GST-ASF1 for binding to full-length CODANIN-1 and its mutants. Full-length CODANIN-1 HMH mutants (R541A, R548A, LL/AA: L545A/L549A), B-domain mutant (B_{mut}: R195A/R196A) and double mutants in HMH and B-domains (R541A+B_{mut}, R548A+B_{mut}, LL/AA+ B_{mut}). **c**, GST-pulldown experiments for the binding of full-length CODANIN-1 using GST-ASF1A or its mutants. Mutants of the HMH binding surface ASF1A (D88A, D54A, V94R), a mutant of the B-domain binding surface in ASF1A (ED/AA: E36A/D37A), double mutants of both HMH and B-domain binding surface in ASF1A (D88+ED/AA, D54A+ED/AA, V94R+ED/AA). Representative gels of the GST pulldown experiments are shown in the left panel and the amount of the binding is quantified in bar graphs in the right panel (royal blue for HMH mutants, cyan for B-domain mutant and purple for double mutants). For all bar graphs, statistical P value was calculated with one-way analysis of variance (ANOVA) (n=3, ns: not significant, *: $p < 0.05$, **: $p < 0.01$, ***: $p < 0.001$, ****: $p < 0.0001$)

CODANIN-1 sequesters ASF1A to prevent its complex formation with histone H3-H4.

We revealed that CODANIN-1 utilizes a histone-mimicking strategy to interact with ASF1, implying that CODANIN-1 and histone H3-H4 are in a competitive relationship toward ASF1A binding. To examine this competitive relationship, we carried out pulldown assays with GST-ASF1A in the presence of histone H3-H4 and increasing amounts of CODANIN-1. These assays showed that histone binding to ASF1a was reduced as CODANIN-1 binding increased (Fig. 4a). This indicates that CODANIN-1 sequesters ASF1A to prevent ASF1A from forming a complex with histone H3-H4. Next, we tested whether CODANIN-1 can deprive ASF1A from the pre-formed ASF1A-H3-H4 complex. We pre-incubated GST-ASF1A with H3-H4 and performed pulldown experiments using the GST-ASF1A_H3-H4 complex with increasing amounts of CODANIN-1 as prey (Fig. 4b and Extended Data Fig. 7). In this setting, while CODANIN-1 still binds to ASF1A_H3-H4, the histone H3-H4 binding to ASF1A was unaffected by CODANIN-1 (Fig. 4b), indicating that CODANIN-1 cannot deprive ASF1A after ASF1A forms a complex with H3-H4, but CODANIN-1 still bind ASF1A-H3-H4 and sequester it.

Figure 4

a

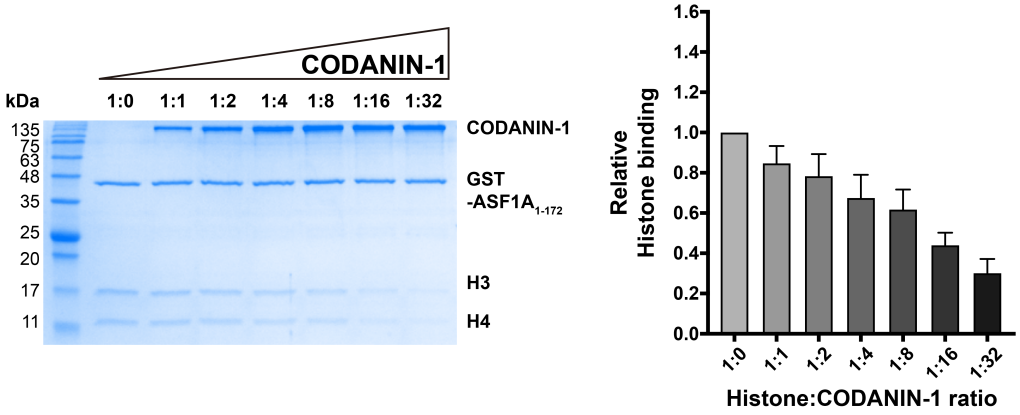

b

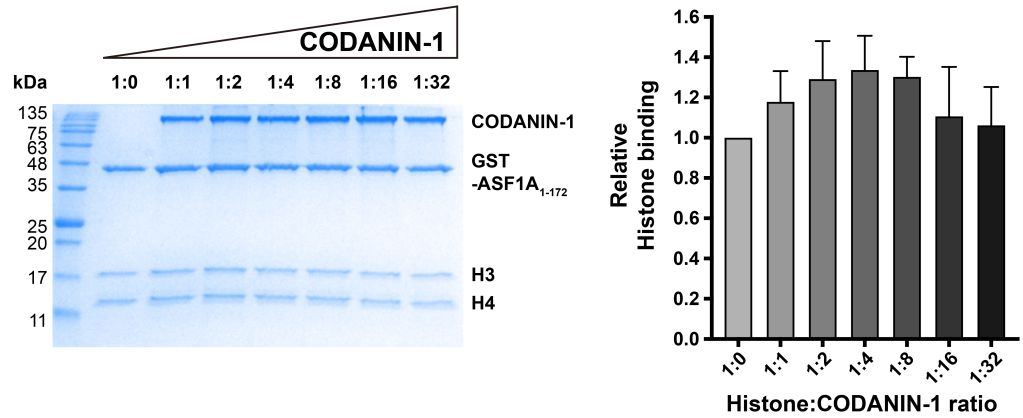

Fig.4 CODANIN-1 sequesters free ASF1A to prevent the complex formation with histone H3-H4. **a,** A representative SDS-PAGE gel of GST-pulldown experiment to verify the competitive relationship between CODANIN-1 and histone H3-H4 (left panel). The ratio of histone H3-H4 to CODANIN-1 is indicated on each gel lane. Quantification of relative histone H3-H4 band intensity to GST-ASF1A band intensity (right panel). The value was normalized by histone H3-H4 band in the absence of CODANIN-1 (1:0 ratio). **b,** A representative SDS-PAGE gel of GST-pulldown experiment to verify histone depriving by the CODANIN-1 (left panel). The ratio of histone H3-H4 to CODANIN-1 is indicated on each gel lane. Quantification of relative histone H3-H4 band intensity to GST-ASF1A band intensity (right panel). The value was normalized to the histone H3-H4 band in the absence of CODANIN-1 (1:0 ratio).

The dimerization of CODANIN-1 is mediated by the second helical lobe and the C-terminal region.

The cryo-EM structure shows that CODANIN-1 forms a homodimer with a large interface (1,844 $Å^2$), which is mediated by the LOBE2 (Fig.1e and Extended Data Fig. 4a,b). Two LOBE2s form a dimer in a saddle joint shape with hydrophobic and electrostatic interactions (Extended Data Fig. 8a). Specifically, at the top of the saddle, the Phe581 residue from each CODANIN-1 is inserted into a hydrophobic pocket formed by Phe581, Met588, Val643, Leu646, and Pro647 from another CODANIN-1 LOBE2 (Fig. 5a and Extended Data Fig.8a). In addition, Arg447 and Glu562 from each molecule makes salt bridges (Fig. 5a). To examine the dimerization interface, we introduced F581E and E652A mutations, disrupting the hydrophobic interaction and the salt bridges. However, unexpectedly, this mutant still forms a dimer (Extended Data Fig. 8b). This observation led us to hypothesized that there may be an additional dimerizing domain in the region not observed in the cryo-EM structure. In our structure, the C-terminal region of CODANIN-1 (819-1,227 a.a.) and CDIN1 are completely disordered. As part of the C-terminal region (1,000-1,227 a.a.) was previously shown to interact with CDIN1[30-32], we envisioned that the C-terminal region of CODANIN-1 or CDIN1 may be involved in CODANIN-1 dimerization in addition to the LOBE2. To examine this possibility, we resorted to AlphaFold2[39] and obtained a predicted model of the C-terminal region (841-1,202 a.a.) of CODANIN-1 complex with full-length of CDIN1 (Extended Data Fig. 9a). The predicted model shows that the C-terminal region of CODANIN-1 forms into two domains. The region of 841-1,000 a.a. forms a coiled-coil structure and the second region of 1,025-1,202 a.a. forms a helical bundle composed of eight α-helices. These two domains are connected by a loop (1,001-1,024 a.a.). The eight helical bundle domain is predicted to form a complex with CDIN1 (Extended Data Fig. 9b). As the domain of 841-1,000 a.a. is predicted to have a coiled-coil structure, we sought the possibility that this coiled-coil domain may form a homo-dimer. Using AlphaFold2, we predicted to generate a dimeric model of the C-terminal region of CODANIN-1 (841-1,202 a.a.) complex with CDIN1. This dimer model shows that two Phe868 residues from each CODANIN-1 make a π-π stacking interaction with their aromatic rings, and Arg864 and Glu871 residues from one molecule make salt bridges with Glu871 and Arg864 from the other molecules respectively (Extended Data Fig. 9c). Interestingly, Phe868 is found to be mutated to Ile868 in CDA-I disease[33], which may disturb the dimerization of the C-terminal region. Based on the predicted model, we generated a dimer mutant (DM_{mut}) having both mutations (F868I/E871R) at the coiled-coil region of CODANIN-1 C-terminal and the mutations (F581E/E652A) at the dimerization interface of the LOBE2. While the mutation in either the dimer interface of LOBE2 or C-terminal coiled-coil region alone does not affect the dimerization of CODANIN-1, the significant portion of the DM_{mut} became monomer (Fig. 5b). Furthermore, negative-stain EM analysis clearly shows that DM_{mut} exhibits smaller size than wild

type CODANIN-1 (Fig. 5b,c and Extended Data Fig. 8b,c). These data suggest that CODANIN-1 has at least two dimerization domains: LOBE2 and the C-terminal region.

The dimerization of CODANIN-1 is not required for ASF1 binding.

Our cryo-EM structure with the predicted model indicates that CODANIN-1 form a dimer through multiple dimerization domains with large interfaces. In addition, CODANIN-1 exhibits a dimer in a gel-filtration chromatography. These observations suggest that CODANIN-1 functions as an obligatory dimer. The dimerization interfaces are located at the opposite end of the ASF1 binding domains. However, it is unclear whether the dimerization of CODANIN-1 is critical for ASF1 binding. Therefore, we collected a fraction containing monomeric CODANIN-1 (DM_{mut}). The monomer state was confirmed by negative stain EM and analytical gel filtration chromatography (Fig. 5b,c and Extended Data Fig. 8c). We then performed GST pulldown analysis with GST-ASF1A with the monomeric CODANIN-1 (Fig. 5d), exhibiting that the monomeric CODANIN-1 showed comparable binding to that of wild type dimeric CODANIN-1 toward ASF1. These data imply that the dimerization of CODANIN-1 is not required for ASF1 binding in-vitro.

Figure 5

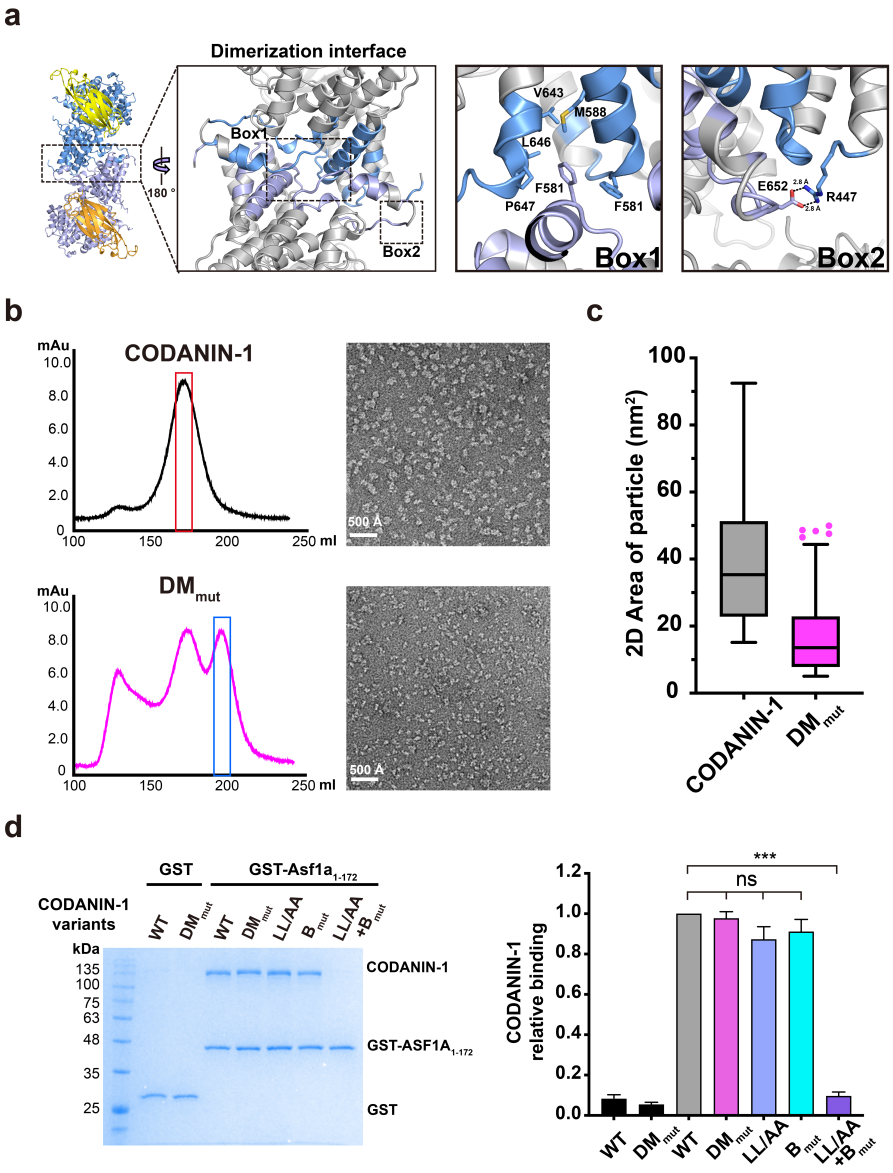

Fig. 5 Dimerization of CODANIN-1 complex.

a, The detailed view of the dimer interface of CODANIN-1 complex. Dashed-line boxes (Box1 and Box2) indicate the dimerization interfaces of CODANIN-1 and the enlarged view of the CODANIN-1 dimerization interface. F581 residue of one CODANIN-1 is inserted into a hydrophobic pocket formed by F581, M588, V643, L646, and P647 residues from the other CODANIN-1 (Box 1). R447 and E652 residues from different CODANIN-1 molecules form a salt bridge (Box 2). **b,** Size-exclusion chromatograms and negative stain EM micrograph images for wild type CODANIN-1 (top panel) and for DM_{mut} (bottom panel). **c,** Box and whisker plot analysis on the 2-dimensional area of the particles (n=339 for WT, n=645 for DM_{mut}) was drawn by Tukey method. **d,** A representative SDS-PAGE gel of GST-pulldown experiment with GST-ASF1A to wildtype, DM_{mut}, HMH mutant (LL/AA: L545A/L549A), B-domain mutant (B_{mut}: R195A/R196A), and double mutant (LL/AA+B_{mut}) (left panel). A bar graph represents the quantification of CODANIN-1 band intensity to the GST-ASF1A band intensity. The value was normalized by band intensity of wildtype CODANIN-1 (right panel). For bar graphs, statistical P value was calculated with one-way analysis of variance (ANOVA) (n=3, ns: not significant, *: $p < 0.05$, **: $p < 0.01$, ***: $p < 0.001$, ****: $p < 0.0001$)

Dual-binding via the HMH and the B-domain is required for CODANIN-1-mediated sequestration of ASF1A in the cytoplasm.

Our cryo-EM structure followed by biochemical analysis identified the interaction mode between CODANIN-1 and ASF1. Next, we aimed to explore the interaction in cells and more specifically towards the ability of CODANIN-1 to sequester ASF1A in the cytoplasm, thereby controlling the flow of newly synthesized histones to chromatin. We utilized the FlpIn system to integrate inducible siRNA resistant CDAN1 constructs into U-2-OS cells as a complementation system[29] (Extended Data Fig. 10a). As CODANIN-1 exhibits low expression in cells, we tagged the mutant constructs with a destabilization domain to keep mutant protein levels low[40]. However, note that even with this approach the complemented proteins were over-expressed compared to endogenous wildtype CODANIN-1. The endogenous protein was depleted by siRNA treatment to address the functionality of CODANIN-1 mutants in the absence of endogenous protein. We validated the knockdown of endogenous CODANIN-1 (Fig. 6a), with siRNA #2 having the strongest effect and therefore being used for the complementation experiments.

To assess the ability of CODANIN-1 mutants to sequester ASF1A in the cytoplasm[29], we assessed the localization of ASF1A in response to knockdown of endogenous CODANIN-1 and complementation with the wildtype or mutant CODANIN-1 (Fig. 6b). We used staining against HA-tagged CODANIN-1 to identify cells with efficient complementation and validated comparable expression levels across the cell lines (Extended Fig. 10b,c). Cells expressing wildtype CODANIN-1 showed a shift in ASF1A to the cytoplasm (Fig. 6c-e) and depletion of ASF1A from the nucleus (Fig. 6f,g), in agreement with its ability to sequester ASF1 in the cytoplasm upon over-expression[29]. Single mutation of the HMH or B-domain also showed cytoplasmic ASF1A signal, but to a slightly lower level than wildtype CODANIN-1, indicating that these domains play a role in ASF1A sequestration. Notably, when the double mutant was expressed, ASF1A remained entirely nuclear (Fig. 6c-e). This demonstrates that the dual-binding mode of CODANIN-1 is required for ASF1A interaction and sequestration in cells. We also examined the effect of CODANIN-1 dimerization on ASF1A binding. The DM_{mut} showed impaired sequestration of ASF1A (Fig. 6d,e), indicating that the dimerization of the CODANIN-1 in some manner influences sequestration in the cytoplasm despite not being directly required for ASF1 binding. This was not related to localization of the DM_{mut}, as this was comparable to wildtype CODANIN-1 (Extended Fig. 10c). The CDA-I disease mutation P672L is located in the dimerization interface, although the mutant still forms a dimer *in vitro* (Extended Data Fig. 8b). Therefore, we also examined the pathogenic P672L mutant for its ability to sequester ASF1A (Fig. 6d,e). This mutant showed a reduction in ASF1a sequestration similar to the DM_{mut} (Fig. 6d,e). In summary, we demonstrate that the dual-binding mode of CODANIN-1 is required for ASF1A binding in cells and its ability to sequester ASF1A in the cytoplasm. We further show that CODANIN-1 dimerization is important for this process, which is also perturbed in a CDA-I mutant.

Figure 6

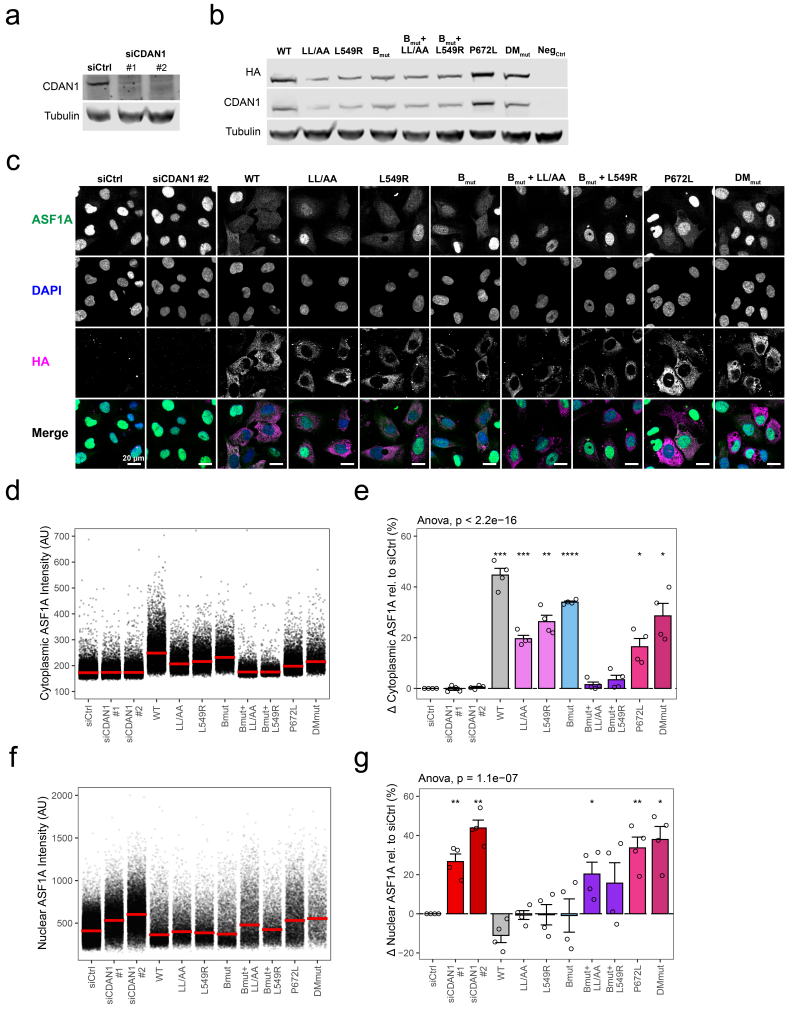

Fig. 6 Dual-binding mode of ASF1A is required for cytoplasmic sequestration by CODANIN-1. **a**, Western blot of endogenous CODANIN-1 after 48 hours siRNA treatment with control siRNA (siCtrl) or siRNA targeting CDAN1 (siCDAN1 #1 and #2). **b**, Western blot showing expression of HA-tagged CODANIN-1 after 24 hours of treatment with doxycycline and Shield1. WT: wild-type, B_{mut}: B domain mutant, DM_{mut}: Dimerisation mutant. **c**, Representative images of ASF1A localization in cell lines expressing exogenous CODANIN-1. siCtrl and siCDAN1 #2 panels represent the parental cell line with control or CDAN1 knockdown respectively. The names of the other panels indicate the exogenous CODANIN-1 mutants. Each cell line was treated with CDAN1#2 siRNA for 48 hours and by doxycycline and Shield1 was added for the last 24 hours to induce expression of exogenous CODANIN-1. **d**, Cytoplasmic ASF1A intensity quantified in individual cells from a single biological replicate as in c. For complementation with exogenous CODANIN-1, only HA-expressing cells were included. Bars show the median and inter-quartile range of each condition. **e**, The relative change in cytoplasmic ASF1A intensity compared to control. For each condition the difference in median cytoplasmic ASF1A intensity compared to the median of siCtrl was calculated (% change). Each dot represents a biological replicate (n=4), and bars and error bars represent the mean±SD. P-values were calculated by one-way ANOVA (* $p<0.05$, ** $p<0.01$, *** $p<0.001$). **f,g,** Nuclear ASF1A intensity quantified in HA-expressing cells using the same methods as in **d,e**. A minimum of 2000 cells were considered per condition, and statistical testing was performed on the median intensities of distinct biological replicates.

Discussion

CODANIN-1 has a unique role as a negative regulator of histone supply by sequestering ASF1[29,41], but the mechanism by which CODANIN-1 sequesters ASF1 remains unknown. Here, we report the atomic resolution cryo-EM structure of the CODANIN-1_ASF1A complex. We find that CODANIN-1 forms a dimer which interacts with two molecules of ASF1A through a dual-binding mode of a HMH and B domain. We demonstrate that CODANIN-1 binds ASF1A in a competitive manner with histones H3-H4 but can also bind a preformed ASF1A-H3-H4 complex, implying two modes for CODANIN-1 regulation of ASF1A activity. We further show that the dual binding mode of CODANIN-1 is essential for cytoplasmic sequestration of ASF1A in cells, demonstrating the importance of this interaction in regulating histone supply. This strengthens our understanding of histone supply regulation and reveals the mechanisms underlying CODANIN-1 control of ASF1A activity.

The structure of the CODANIN-1_ASF1A complex reveals two ASF1A binding motifs in CODANIN-1: the HMH helix and the B-domain. These two motifs are highly conserved among species (Extended Data Fig. 3), implying conservation and functional importance to ASF1A regulation by CODANIN-1. This dual binding mode occludes both the major interaction sites of ASF1A, reminiscent of early work hinting towards a similar mechanism mode of Rad53 interaction with yeast Asf1[42] which would be interesting to revisit in light of our findings. CODANIN-1 binding would both prevent the interaction of ASF1A with histones via the HMH and with other chaperones by the B-domain, thereby sequestering ASF1A in a fully inactive state. Consistent with the importance of dual-binding for ASF1A inactivation, mutation of both the HMH and B-domain is required to fully prevent ASF1A sequestration. Our BLI data shows that CODANIN-1 binds with picomolar-scale apparent dissociation constant showing the very strong binding of ASF1A. Considering that ASF1A sequestration should be dynamic in order to regulate histone supply in response to stimuli, it would be interesting to examine whether there is a regulatory mechanism, yet to be identified, to release ASF1A from CODANIN-1. The fact that CODANIN-1 has the HMH occupying the histone binding surface of ASF1A implies that CODANIN-1 would prevent ASF1A from forming a histone complex. It would also prevent the binding of TLK2, which binds through a similar mechanism using a histone mimicking motif[43] and is involved in positive regulation of histone supply. Therefore, CODANIN-1 HMH binding would act as a strong inhibitor of ASF1-mediated histone supply, preventing both the activating phosphorylation by TKL2 and histone binding. DNAJC9 is suggested to support ASF1 in histone supply[12] and it would be an interesting area of future discovery to investigate how ASF1 inactivation by CODANIN-1 affect the activities of DNAJC9 and other supply chaperones in the histone supply chain.

The B-domain is also found in other ASF1A binding proteins such as CAF-1 and HIRA[27,28,42,44,45] and the binding mode of the CODANIN-1 B-domain to ASF1A is similar to these

downstream chaperones. Interestingly, in our cryo-EM structure the B-domain (193-203 a.a.) is the only structured part among a large disordered region (69-284 a.a.), suggesting the B-domain likely becomes ordered upon the interaction with ASF1A. Therefore, without ASF1A binding, the entire region (69-284 a.a.) containing the B-domain would be flexible. It is plausible that this large loop may fish free ASF1A to be tethered to CODANIN-1, as it can bind ASF1A independent of the HMH. As CODANIN-1 can also bind ASF1A already bound to a histone dimer (Fig. 4b), this raises the possibility that B domain binding by CODANIN-1 could be a mechanism to regulate ASF1A delivery of histones to downstream chaperones. This could not only be used to sequester histone-bound ASF1A outside of the nucleus, as by cytoplasmic CODANIN-1 prominent for the over-expressed protein (Fig. 6c), but may also be a function of the endogenous nuclear pool of CODANIN-1 which predominantly localizes to the nucleolus[46]. CODANIN-1 binding to ASF1A-H3-H4 would inhibit the handover of histones to downstream B-domain containing chaperones such as CAF-1 and HIRA. This could lead to sequestration of ASF1A-H3-H4 in the nucleus and to provide a more dynamic mechanism for regulating histone supply by acting as a downstream of histone import. This may be especially important in conditions where histone supply must be strongly inhibited, for example during erythrocyte differentiation and enucleation where excess delivery of acetylated histones might counteract the histone deacetylation[47,48] and removal[49,50] critical for the process. The identification of the CODANIN-1_ASF1 binding mode now opens an avenue for structure-function studies to address how this inhibitory axis feeds into functions of chaperones such as CAF-1, HIRA, and DNAJC9 in different cell types.

In the cryo-EM structure, a large portion of the C-terminal region of CODANIN-1 and CDIN1 are not visible, suggesting that the C-terminal region of CODANIN-1, known to interact with CDIN1, is dynamic. Interestingly, our structural and biochemical analysis on the C-terminal region revealed that the C-terminal region is also involved in CODANIN-1 dimerization. Mutations in CODANIN-1 and CDIN1 causes CDA-1 disease, suggesting that they function in a same functional axis[33,34,46,51]. However, CODANIN-1 alone is sufficient to bind ASF1 in our in-vitro binding assay. The contribution of CDIN1 to CODANIN-1 function in regulation of histone supply is thus unclear and further structural and mechanistic studies will be required to illuminate CDIN1 function. However, pathogenic mutations involved in CDA-I occur most often towards the C-terminus in the large dimerization domain of CODANIN-1, and in CDIN1[46]. CODANIN-1 interacts with CDIN1 through the C-terminal domain (1,001-1,227 a.a.), which contains the R1042W mutant previously shown to contribute to ASF1A sequestration[29]. The pathogenic mutations P672L and dimerization mutants assessed in this study show a similar reduction in the ability to sequester ASF1A. The prevalence of disease-causing mutations in the dimerization and CDIN1 interaction interface, along with the reduction in ASF1A sequestration from pathogenic mutant CODANIN-1, may suggest that defect in the integrity of CODANIN-1_CDIN1 complex contributes to CDA-I development at least in

part through inefficient regulation of ASF1A. The spongy heterochromatin and nuclear abnormalities of CDA-I[35,37,52] could also suggest that defective chromatin regulation may underly the disease. This could be due to an inability to sequester ASF1A outside the nucleus, or by altering the interactions of ASF1A with other chaperones within the nucleus. CODANIN-1_CDIN1 could also have further unexplored activities which could contribute to disease pathogenesis, for example the DNA binding or nuclease activities first suggested for CDIN1 by sequence similarity[34]. Further structure-function exploration of CODANIN-1_CDIN1 complex, and its roles in and beyond in chromatin regulation in hematopoiesis will be important for understanding and treating CDA-I.

Acknowledgement

We thank the members of Song lab for helpful discussion. We thank KAIST Analysis Center for Advanced Research (KARA), Institute of Membrane Proteins (IMP), Research Resource Center at Institute of Basic Science (IBS), and Global Science Data Center (GSDC) at Korea Institute of Science and Technology Information (KISTI) for supporting cryo-EM facilities and computing resources. This work is partially supported by grants (RS-2024-00333346, RS-2023-00266300 to J.S.) by National Research Foundation of Korea and Grand Challenge 30 by KAIST. T.K. is supported by Brain Korea 21 program. Research in A.G.'s laboratory was supported by the Novo Nordisk Foundation (NNF21OC0067425) and the European Research Council (CoG 724436). Research at CPR is supported by the Novo Nordisk Foundation (NNF14CC0001).

Data availability

The cryo-EM map was deposited to EMDB (ID: EMD-60697) and the coordinates of the atomic structure to PDB (ID: 9IMZ).

Declaration of Conflict of Interest

J.S. is a CTO of Epinogen. A.G. is a co-founder and CSO of Ankrin Therapeutics. All other authors declare that they have no competing interests.

Methods

Purification of CODANIN-1 complex

CODANIN-1 and CDIN1 were cloned into a pFastBac1 vector with a C-terminal 6xHis tag and a TEV protease cleavage site (ENLYFQG) before the His tag for CODANIN-1, and with no tag for CDIN1. The cloned plasmids were transformed into DH10Bac competent cells to generate bacmid DNAs. Bacmid DNAs were transfected into *Spodoptera frugiperda* 9 (Sf9) cells to produce baculoviruses harboring CODANIN-1 and CDIN1. These baculoviruses were amplified to passage 3 according to the Bac-to-Bac Baculovirus Expression Kit (Thermo Fisher Scientific). The two baculoviruses were co-infected into Sf9 cells and harvested 48 hours post-infection in a lysis buffer (50 mM Tris, pH 8.0, 500 mM NaCl, 5% glycerol) containing a protease inhibitor cocktail (Roche).The Sf9 cells were lysed by repeated freezing and thawing cycles and cell debris were cleared with a centrifugation at 27,216 g for 2 hrs. ASF1a$_{1-172}$ was cloned into pET21a vector with no tag and was expressed from *Escherichia coli (E. coli)* BL21 Codon Plus(DE3)-RILP. The bacteria cells were harvested in a lysis buffer and lyzed by sonication and the debris were cleared with a centrifugation at 27,216 g for 2 hours. The prepared Sf9 and bacteria cell lysates were mixed and the mixture was loaded into Ni-NTA resin (Qiagen) packed gravity-flow column. The column was washed with a washing buffer (50 mM Tris pH 8.0, 500 mM NaCl, 5% glycerol, 20 mM Imidazole) and the bound protein was eluted with an elution buffer (50 mM Tris pH 8.0, 500 mM NaCl, 5% glycerol, 150 mM Imidazole). The eluted sample was then diluted up with the four volume of the sample with 50 mM Tris HCl pH8.0 and loaded into HiTrap Q HP (Cytiva). The protein was eluted with a salt gradient from 0 to 1 M NaCl. The fraction containing CODANIN-1 complex was further purified with a size exclusion chromatography (HiLoad 16/600 Superose 6 pg (Cytiva)) equilbriated with a buffer (50 mM Tris pH8.0, 500 mM NaCl, 5% glycerol). The fractions containing CODANIN-1_ASF1A_CDIN1 fractions were collected and concentrated by Amicon Ultra Centrifugal Filter 100 kDa MWCO (Merck Millipore) up to 3mg/mL. The sample was stored at -80°C after flash-freezing into liquid nitrogen. CODANIN-1 mutants were purified similarly.

Cryo-EM structure determination

To determine the cryo-EM structure of the CODANIN-1 complex, the complex was further separated with a GraFix method as previously described[53]. Briefly, the sample was separated by sucrose gradient ultracentrifugation with the gradients of 10 to 30 % sucrose and 0 to 0.2 % glutaraldehyde at 97,311 g at 4°C for 18hrs using an Optima™ XL-100K ultracentrifuge (Beckman Coulter). The fractions containing the complex were pooled and the sucrose was removed by using Amicon Ultra Centrifugal Filter, 100 kDa MWCO, 0.5ml (Merck Millipore). The sample was then loaded on a graphene oxide covered (homemade) holey carbon grid (Quantifoil R1.2/1.3, copper, 300 mesh) and

plunge-frozen using a Vitrobot Mark IV (FEI/Thermo Fisher Scientific) under 100% humidity at 15°C with -13 blotting force and 3 sec blotting time. The micrographs were collected using a Titan Krios G4 300 keV Transmission Electron Microscope (Thermo Scientific) equipped with a BioQuantum K3 detector (Gatan) at Institute of Membrane Proteins (IMP). Total 4,282 micrographs were collected with parameters of 1.1 apix, 58.9 e/Å^2 total electron dose over 50 frames, 18 eV of energy filter slit width, and defocus range of -0.8 μm to -2.4 μm (0.2 μm/steps). The data were processed with CryoSPARC v4.2.1[54]. The micrographs were preprocessed with Full-Frame Motion Correction and CTFFIND4 embedded in CryoSPARC[55,56]. The total of 4,075 micrographs were selected based on the proper defocus value, the degree of astigmatism and the motion distance and curvature. From the selected micrographs, particles were picked by blob-picking followed by template-based picking and subjected to four rounds of 2D classification. 36,361 good particles were selected and used as a training data set for Topaz picking[57]. Out of the total 1,592,796 particles picked, 524,649 particles were selected for reconstructing initial models and for 3D classification. After iterative 3D classification, final 111,999 particles were used for reconstructing 4.66 Å resolution cryo-EM map of CODANIN-1 complex with C2 symmetry. After local motion correction[58] and 3D refinement, the final map reached at 3.56 Å resolution calculated by gold-standard Fourier shell correlation (cut-off at 0.143). Map sharpening was automatically operated in CryoSPARC 3D refinement with calculated B-factor. Local resolution map was generated in CryoSPARC local resolution estimation.

To evaluate the potential for artifacts introduced by C2 symmetry expansion, we re-analyzed the cryo-EM data without applying symmetry. Through an additional round of 3D classification, we got a refined dataset comprising 56,039 particles. Subsequent processing steps included local motion correction, CTF refinement, and non-uniform refinement, we finally generated a cryo-EM density map at 3.78 Å resolution[58-60] (Extended Data Fig. 1a). This map exhibited structural similarity to the CODANIN-1 complex structure with C2 symmetry, indicating that the C2 symmetry applied structure is not an artifact.

The atomic model was built based on final refinement map. The structure of ASF1A (PDB ID 2IO5) was used as a initial model for ASF1A[26]. This model was manually fitted into the density map using ChimeraX[61]. Subsequently, manual rebuilding with Cα tracing and side chain fitting was performed in Coot[62] and adjusted through rigid-body refinement in Phenix[63] . This was followed by real-space refinement in Phenix, incorporating minimization global, local grid search, ADP, occupancy refinement with secondary structure restraints and Ramachandran restraints. Iterative adjustments were then made to eliminate Ramachandran outliers, Rotamer outliers and Cβ outliers, and to improve the model geometry by coot and Isolde 1.3[64]. The final statistics (Table 1) were calculated through comprehensive validation in Phenix.

Protein expression

We generated GST fusion peptides for HMH (CODANIN-1 520-557 a.a.) and its mutants (R541A, R448A, LL/AA: L545A/L549A), as well as for the B-domain (CODANIN-1 183-217 a.a.) and its mutant (B_{mut} : R195A/R196A) clones, using a modified version of the pET22b vector (Novagen). Subsequently, to expressed all of GST-fused HMH and mutants and GST-fused B-domain and mutant, each clone was transformed into E. coli strain BL21 Codon Plus (DE3)-RILP cells. The cells were cultured in a shaking incubator at 37°C and 180rpm. Upon reaching an OD600 of 0.6, IPTG was added to a final concentration of 0.5 mM for induction. Following induction, for all cell batches were cultured for 3 hours and then harvested in lysis buffer (50 mM Tris, pH 8.0, 500 mM NaCl, 5% glycerol, 1 mM PMSF). Sonication was employed to lyse the cells, and subsequent removal of cell debris by centrifugation at 27,216 g for 1 hour. For the prepared bacterial cell lysates, 2mL of Glutathione Sepharose 4B resin (Cytiva) was added and incubated at 4°C for 2 hours on a tube roller mixer. Consequently, four times of washing with wash buffer (50 mM Tris, pH 8.0, 500 mM NaCl, 5% glycerol) followed by the resin loading into gravity-flow column. The column was washed with a washing buffer (50 mM Tris pH 8.0, 500 mM NaCl, 5% glycerol) and the bound protein was eluted with an elution buffer (50 mM Tris pH 8.0, 150 mM NaCl, 5% glycerol, 10 mM Glutathione reduced). The eluted sample was then diluted up with the three volume of the sample with 50 mM Tris HCl pH8.0 and loaded into HiTrap Q HP (Cytiva). The protein was eluted with a salt gradient from 0 to 1 M NaCl. The fractions containing GST fusion HMH or GST fusion B-domain were collected and concentrated by Amicon Ultra Centrifugal Filter 10 kDa MWCO (Merck Millipore) up to 3 mg/mL. The sample was stored at -80°C after flash-freezing into liquid nitrogen.

For the GST fusion $ASF1A_{1-172}$, we cloned truncated ASF1A (1-172 a.a.) into pGEX-4T-1 vector. Following this, we introduced mutations on the HMH and B-domain interaction surface of ASF1A: D88A, D54A, V94R for HMH interaction, E36A/D37A (ED/AA) for B-domain interaction. To expressed GST_$ASF1A_{1-172}$ and its mutants, we transformed these clones into E. coli strain BL21 Codon Plus (DE3)-RILP cells. The protein expression and preparation steps were identical to those used for the aforementioned GST fusion peptides. GST-ASF1A variants were concentrated using Amicon Ultra Centrifugal Filter 30 kDa MWCO (Merck Millipore) to a 2.5 mg/mL. The concentrated proteins were then flash-frozen in liquid nitrogen and stored at -80°C.

GST pulldown assay

To verify the interaction between HMH and ASF1A, as well as between the B-domain and ASF1A, we conducted a GST pulldown assay. In this assay, 25 µl of Glutathione Sepharose 4B resin (Cytiva) was mixed with 125 µg of purified GST fusion HMH or B-domain in a total 500 µl volume of incubation buffer (50 mM Tris, pH 8.0, 150 mM NaCl, 5% glycerol). The mixture was incubated at 4°C for 2 hours on a tube roller mixer. The beads were then washed four times with wash buffer (50

mM Tris, pH 8.0, 150 mM NaCl, 5% glycerol, 0.5% Triton X-100), followed by the addition of 150 μg of $ASF1A_{1-172}$ in a total volume of 500 μl of incubation buffer. This mixture was incubated for 2 hours at 4°C on a tube roller mixer. Post-incubation, the beads underwent four washes with wash buffer to eliminate non-specific binding. Following this, SDS sample buffer was added, and SDS-PAGE was performed using a 16% acrylamide gel. The intensity of the ASF1A bands was measured using Image Lab Software (Bio-Rad). The GST pulldown assays for HMH and B-domain mutants were conducted in the same manner.

To verify the interaction between full-length CODANIN-1 and its mutants with ASF1A, we designed a GST pulldown assay. In this assay, 25 μl of Glutathione Sepharose 4B resin (Cytiva) was mixed with purified GST fusion ASF1A and CODANIN-1 to reach a final concentration of 100 nM each in a total 500 μl volume of incubation buffer (50 mM Tris, pH 8.0, 500 mM NaCl, 5% glycerol). The mixture was then incubated at 4°C for 2 hours on a tube roller mixer. The beads were washed four times with wash buffer (50 mM Tris, pH 8.0, 500 mM NaCl, 5% glycerol, 0.5% Triton X-100), and SDS sample buffer was added to denature the proteins. SDS-PAGE was carried out using a 10% acrylamide gel, and the gel intensity was measured using Image Lab Software (Bio-Rad). The GST pulldown assays for mutant ASF1A and CODANIN-1 were conducted in the same manner.

To verify the competitive relationship between CODANIN-1 and histone H3-H4 over the ASF1 binding, we conducted GST pulldown-based competition assay. In this assay, 25μl of Glutathione Sepharose 4B resin (Cytiva) was mixed with a final concentration of 100 nM purified GST fusion ASF1A in a total volume of 500 μl incubation buffer (50 mM Tris, pH 8.0, 500 mM NaCl, 5% glycerol). Subsequently, histone H3-H4 was added to a final 100nM, and CODANIN-1 was added at doubling molar ratios ranging from 0 to 32 times that of histone H3-H4 (0 nM to 3200 nM). The mixture was incubated for 2 hours at 4°C on a tube roller mixer. Following incubation, the resin was washed four times with wash buffer (50 mM Tris, pH 8.0, 500 mM NaCl, 5% glycerol, 0.5% Triton X-100), and SDS sample buffer was added to denature the proteins. SDS-PAGE was carried out using a 10% acrylamide gel, and the gel intensity was measured using Image Lab Software (Bio-Rad).

In the histone depriving assay, we utilized a final 100 nM of the pre-formed GST-ASF1A and histone H3-H4 complex as a bait, instead of free-ASF1A. CODANIN-1 was subsequently added at doubling molar ratios, ranging from 0 nM to 3200 nM (0 to 32 times the concentration of histone H3-H4). The remaining conditions were identical to those described in the aforementioned competition assay.

Biolayer interferometry (BLI)

We employed purified 6xHis-tagged $ASF1A_{1-172}$ as the ligand and CODANIN-1 variants, including wildtype and mutants (LL/AA: L545A/L549A, B_{mut}: R195A/R196A, LL/AA+B_{mut}) as analytes. Each

sample was stored in a working buffer (50 mM Tris, pH 8.0, 500 mM NaCl, 1X kinetics buffer Octet Kinetics Buffer (Sartorius)). BLI measurements were conducted using the Octet R8 (sartorius). Initially, a baseline was established for 60 seconds using the working buffer. Following this, 4 µM of 6xHis-tagged ASF1A$_{1-172}$ was immobilized on nickel-charged tris-nitriloacetic acid (Tris-NTA) biosensor (Sartorius) for the 90 seconds. A second baseline was then established for 60 seconds with the working buffer. Subsequently, the CODANIN-1 variants were introduced during a 240-second association step. Finally, the biosensor was immersed in the washing buffer for a 480-second dissociation step. To determine the binding kinetics, CODANIN-1 underwent seven BLI runs with serial dilutions ranging from 512 nM to 8 nM. Binding kinetics were analyzed by the Octet BLI Analysis 12.2.2.4 software package (Sartorius).

Cell culture

U2OS cells were cultured in Dulbecco's Modified Eagle Medium (Gibco) supplemented with 10% FBS and 1% penicillin/streptomycin. Cells were passaged every 4-6d when they reached approximately 80% confluency. FlpIn U2OS cells containing the mutant CDAN1 constructs were maintained with 100 µg/ml hygromycin.

Mutant CDAN1 Plasmid Generation

A plasmid containing siRNA-resistant FLAG-HA-CDAN1 cDNA(Ask et al., 2012) on an FRT/TO backbone for Flippase integration was used as the original template. The Shield-1 destabilization domain was fused to the N-terminus after the FLAG-HA tag by megaprimer cloning and the resulting construct was sequenced to check for mutations. Q5 PCR-based site-directed mutagenesis was then used to introduce each point mutation, where back to back primers were used to amplify the whole plasmid and introduce a mutation. Primers were designed using NEBasechanger and are listed in Supplementary Table 3. PCR was performed according to manufacturer instructions with an annealing temperature of 72C. 1µl of PCR product was treated with 1µl T4 PNK, 1µl T4 PNK buffer (NEB) supplemented with 10 mM ATP and 1µl DpnI (NEB) for 1 hour, before adding 1µl Quick Ligase for 15 min prior to transformation of Top10 bacteria. Colonies were picked and plasmids extracted by MiniPrep kit (Qiagen) and the mutation sites were sequenced to confirm successful integration. Sanger sequencing was performed by Eurofins Genomics TubeSeq service and a list of plasmids generated is available in Supplementary Table 2.

Transfection and selection

$5x10^5$ U2OS cells were seeded in wells of a 6-well plate 24 hours prior to transfection. Medium was replaced with fresh medium prior to transfection. Transfection was performed using Lipofectamine 3000 (ThermoFisher), with 250ng of FRT/TO plasmid and 2 µg of pOG44 containing Flippase.

Control wells containing FRT/TO plasmid or pOG44 alone were also transfected, along with an untransfected control. Transfection medium was replaced after 24 hours for full medium. 24 hours later, cells were seeded on a 10cm plate with 200 µg/ml hygromycin, and hygromycin-containing medium was replaced every 3-4d until complete death of the control cells.

siRNA transfection

siRNA transfections were performed with Lipofectamine RNAimax (ThermoFisher) according to manufacturer instructions. siRNAs were added to a final concentration of 10nM. For western blot, the siRNA mix was added dropwise to the well 48 hours prior to harvesting. For the transfections in 96-well plates for microscopy, the siRNA mix was added to each well before seeding, 48 hours before fixation. Control siRNA (siCtrl) used was MISSION siRNA Universal Negative Control #1 (Sigma, SIC001). The CDAN1-targeting siRNAs were siCdan1 #1 (Sigma): 5′-CGUAGAGUUCGUGGCAGAAAGAAUU-3′ (sense strand), siCdan1 #2: ON-TARGET plus SMART pool (Dharmacon).

Western Blot

$2x10^5$ U2OS cells were seeded 48 hours prior to siRNA transfection in 6-well plates. siRNA treatment was performed 48 hours prior to harvest. In the complementation cell lines, expression of the CDAN1 construct was induced with 100 ng/µl doxycycline and 50nM Shield1 for 24 hours prior to harvesting. Cells were harvested by washing 2x in cold PBS and lysing in 50 µl Laemmli sample buffer (50 mM Tris-Hcl pH 6.8, 4% SDS, 10% glycerol, 0.1% bromophenol blue, and 25 mM DTT) and treated for 1 hour with 1 µl of benzonase and 0.5 µl of 1M MgCl2. 5 µl of protein lysate was separated by gel electrophoresis on a NuPAGE 4-12% Bis-Tris Gel (ThermoFisher) and transferred by semi-dry transfer in NuPAGE transfer buffer (ThermoFisher) supplemented with 20% ethanol. Transfer efficiency was assessed by Ponceau staining. Membranes were blocked in 5% milk in phosphate-buffered saline with 0.01% tween-20 (PBST) for 1 hour at room temperature, before being incubated with antibodies in milk overnight at 4°C. Membranes were washed 3x in PBST before incubating for 1 hour with secondary antibodies at RT. Secondary antibodies used were IRDye 680RD Goat anti-Mouse IgG and IRDye 800CW Goat anti-Rabbit IgG (Licor). Once the secondary antibodies were added, all incubations were performed in the dark. After secondary incubation, the membranes were washed 3x in PBST and imaged using a LiCOR Odyssey M. All western blots were performed with 2 biological replicates.

Microscopy

7.5 x10^4 U2OS cells resuspended in 150 µl of medium were added to each well of a 96 well plate containing 50 µl of siRNA transfection mix. Medium was replaced with new medium containing 100 ng/µl doxycycline and 50nM Shield1 24 hours prior to harvest. Cells were fixed 48 hours after seeding. To fix, the plates were washed in cold PBS and incubated with 4% paraformaldehyde (PFA) for 15 minutes. PFA was removed and the plates washed 3x in PBS. Wells were filled with 100 µl of cold PBS, sealed with parafilm, and kept in the fridge until further processing. Each experiment was performed with 4 biological replicates with cells cultured separately for a minimum of 2 passages. Cells were permeabilized in 0.5% Triton-X for 15 minutes. All incubation steps were performed with gentle shaking. Each well was then washed 2x with PBS before incubation in 100 µl of blocking buffer (5% BSA, 0.1% Triton-X) for 1 hour at RT. Cells were incubated with primary antibody in blocking buffer overnight at 4°C. The next day wells were washed 3x with blocking buffer, before incubating with secondary antibodies for 1 hour at RT in the dark. Secondary antibodies used were Alexa-488 anti-Rabbit and Alexa 568 anti-Mouse (Invitrogen). Wells were washed 2x in blocking buffer and 1x in PBS, before incubation in 4′,6-diamidino-2-phenylindole (DAPI). 2x PBS washes were then performed and each well was kept in 100 µl PBS until imaging. Imaging was performed using an Opera Phenix Plus with a 40x objective.

Image Analysis

Nuclei segmentation, cytoplasm detection, and fluorescence intensity measurements were performed using Harmony 4.9 software. Intensity measurements for each cell were exported from the Harmony software for analysis and visualization using RStudio 4.3. For complementation cell lines, the expression of the mutant protein was defined based on a higher HA intensity in the cytoplasm compared to the parental cell line which does not express HA-tagged proteins. Only HA-positive cells were used in the analysis for the complementation cell lines. Images for visualization were exported to ImageJ, where brightness and contrast were edited for visibility without altering pixel values. All images were processed using the same steps. Figures with visualizations were prepared using QuickFigures[65].

Statistics

Statistical tests on microscopy data were performed between the medians of multiple biological replicates. For comparisons between multiple conditions, paired ANOVA was used paired by the replicate. When the ANOVA showed a difference between conditions, paired t-test was used to find the difference between specific conditions. Significance threshold was defined as $p<0.05$.

REFERENCES

1. Luger, K., Mäder, A.W., Richmond, R.K., Sargent, D.F. & Richmond, T.J. Crystal structure of the nucleosome core particle at 2.8 Å resolution. *Nature* **389**, 251-260 (1997).
2. Bannister, A.J. & Kouzarides, T. Regulation of chromatin by histone modifications. *Cell Research* **21**, 381-395 (2011).
3. Li, B., Carey, M. & Workman, J.L. The role of chromatin during transcription. *Cell* **128**, 707-19 (2007).
4. Kornberg, R.D. & Lorch, Y. Twenty-five years of the nucleosome, fundamental particle of the eukaryote chromosome. *Cell* **98**, 285-294 (1999).
5. Groth, A., Rocha, W., Verreault, A. & Almouzni, G. Chromatin challenges during DNA replication and repair. *Cell* **128**, 721-33 (2007).
6. Lai, W.K.M. & Pugh, B.F. Understanding nucleosome dynamics and their links to gene expression and DNA replication. *Nature Reviews Molecular Cell Biology* **18**, 548-562 (2017).
7. Teves, S.S., Weber, C.M. & Henikoff, S. Transcribing through the nucleosome. *Trends Biochem Sci* **39**, 577-86 (2014).
8. Groth, A. et al. Human Asf1 regulates the flow of S phase histones during replicational stress. *Mol Cell* **17**, 301-11 (2005).
9. Corpet, A. et al. Asf1b, the necessary Asf1 isoform for proliferation, is predictive of outcome in breast cancer. *The EMBO Journal* **30**, 480-493 (2011).
10. Jasencakova, Z. et al. Replication Stress Interferes with Histone Recycling and Predeposition Marking of New Histones. *Molecular Cell* **37**, 736-743 (2010).
11. Campos, E.I. et al. The program for processing newly synthesized histones H3.1 and H4. *Nat Struct Mol Biol* **17**, 1343-51 (2010).
12. Hammond, C.M. et al. DNAJC9 integrates heat shock molecular chaperones into the histone chaperone network. *Mol Cell* **81**, 2533-2548.e9 (2021).
13. Ai, X. & Parthun, M.R. The Nuclear Hat1p/Hat2p Complex: A Molecular Link between Type B Histone Acetyltransferases and Chromatin Assembly. *Molecular Cell* **14**, 195-205 (2004).
14. Barman, H.K. et al. Histone acetyltransferase-1 regulates integrity of cytosolic histone H3-H4 containing complex. *Biochem Biophys Res Commun* **373**, 624-30 (2008).
15. Yoon, J. et al. Integrative Structural Investigation on the Architecture of Human Importin4_Histone H3/H4_Asf1a Complex and Its Histone H3 Tail Binding. *Journal of Molecular Biology* **430**, 822-841 (2018).
16. Bernardes, N.E., Fung, H.Y.J., Li, Y., Chen, Z. & Chook, Y.M. Structure of IMPORTIN-4 bound to the H3–H4–ASF1 histone–histone chaperone complex. *Proceedings of the National Academy of Sciences* **119**, e2207177119 (2022).
17. Tyler, J.K. et al. The RCAF complex mediates chromatin assembly during DNA replication and repair. *Nature* **402**, 555-560 (1999).
18. Mello, J.A. et al. Human Asf1 and CAF-1 interact and synergize in a repair-coupled nucleosome assembly pathway. *EMBO reports* **3**, 329-334-334 (2002).
19. Ray-Gallet, D. et al. HIRA is critical for a nucleosome assembly pathway independent of DNA synthesis. *Mol Cell* **9**, 1091-100 (2002).
20. Tagami, H., Ray-Gallet, D., Almouzni, G. & Nakatani, Y. Histone H3.1 and H3.3 complexes mediate nucleosome assembly pathways dependent or independent of DNA synthesis. *Cell* **116**, 51-61 (2004).
21. Loppin, B. et al. The histone H3.3 chaperone HIRA is essential for chromatin assembly in the male pronucleus. *Nature* **437**, 1386-1390 (2005).
22. Groth, A. et al. Regulation of replication fork progression through histone supply and demand. *Science* **318**, 1928-31 (2007).

23. Sanematsu, F. et al. Asf1 Is Required for Viability and Chromatin Assembly during DNA Replication in Vertebrate Cells*. *Journal of Biological Chemistry* **281**, 13817-13827 (2006).
24. Schulz, L.L. & Tyler, J.K. The histone chaperone ASF1 localizes to active DNA replication forks to mediate efficient DNA replication. *The FASEB journal* **20**, 488-490 (2006).
25. English, C.M., Adkins, M.W., Carson, J.J., Churchill, M.E.A. & Tyler, J.K. Structural Basis for the Histone Chaperone Activity of Asf1. *Cell* **127**, 495-508 (2006).
26. Natsume, R. et al. Structure and function of the histone chaperone CIA/ASF1 complexed with histones H3 and H4. *Nature* **446**, 338-341 (2007).
27. Tang, Y. et al. Structure of a human ASF1a-HIRA complex and insights into specificity of histone chaperone complex assembly. *Nat Struct Mol Biol* **13**, 921-9 (2006).
28. Malay, A.D., Umehara, T., Matsubara-Malay, K., Padmanabhan, B. & Yokoyama, S. Crystal Structures of Fission Yeast Histone Chaperone Asf1 Complexed with the Hip1 B-domain or the Cac2 C Terminus*. *Journal of Biological Chemistry* **283**, 14022-14031 (2008).
29. Ask, K. et al. Codanin-1, mutated in the anaemic disease CDAI, regulates Asf1 function in S-phase histone supply. *Embo j* **31**, 2013-23 (2012).
30. Shroff, M., Knebel, A., Toth, R. & Rouse, J. A complex comprising C15ORF41 and Codanin-1: the products of two genes mutated in congenital dyserythropoietic anaemia type I (CDA-I). *Biochemical Journal* **477**, 1893-1905 (2020).
31. Swickley, G. et al. Characterization of the interactions between Codanin-1 and C15Orf41, two proteins implicated in congenital dyserythropoietic anemia type I disease. *BMC Molecular and Cell Biology* **21**, 18 (2020).
32. Stojaspal, M. et al. Structural insights into inherited anemia CDA-I: disease-associated mutations disrupt CDIN1-Codanin1 complex. *bioRxiv*, 2023.05.25.542057 (2023).
33. Dgany, O. et al. Congenital Dyserythropoietic Anemia Type I Is Caused by Mutations in Codanin-1. *The American Journal of Human Genetics* **71**, 1467-1474 (2002).
34. Babbs, C. et al. Homozygous mutations in a predicted endonuclease are a novel cause of congenital dyserythropoietic anemia type I. *Haematologica* **98**, 1383-7 (2013).
35. Heimpel, H., Forteza-Vila, J., Qveisser, W. & Spiertz, E. Electron and Light Microscopic Study of the Erythroblasts of Patients With Congenital Dyserythropoietic Anemia. *Blood* **37**, 299-310 (1971).
36. Noy-Lotan, S. et al. Cdan1 Is Essential for Primitive Erythropoiesis. *Frontiers in Physiology* **12**(2021).
37. Noy-Lotan, S. et al. Codanin-1, the protein encoded by the gene mutated in congenital dyserythropoietic anemia type I (CDAN1), is cell cycle-regulated. *Haematologica* **94**, 629 (2009).
38. Carraro, M. et al. DAXX adds a de novo H3.3K9me3 deposition pathway to the histone chaperone network. *Mol Cell* **83**, 1075-1092.e9 (2023).
39. Jumper, J. et al. Highly accurate protein structure prediction with AlphaFold. *Nature* **596**, 583-589 (2021).
40. Haugwitz, M., Garachtchenko, T., Nourzaie, O., Gandlur, S. & Sagawa, H. Rapid, on-demand protein stabilization and destabilization using the ProteoTuner™ systems. *Nature Methods* **5**, iii-iv (2008).
41. Hammond, C.M., Strømme, C.B., Huang, H., Patel, D.J. & Groth, A. Histone chaperone networks shaping chromatin function. *Nature Reviews Molecular Cell Biology* **18**, 141-158 (2017).
42. Jiao, Y. et al. Surprising complexity of the Asf1 histone chaperone-Rad53 kinase interaction. *Proc Natl Acad Sci U S A* **109**, 2866-71 (2012).

43. Simon, B. et al. Tousled-like kinase 2 targets ASF1 histone chaperones through client mimicry. *Nat Commun* **13**, 749 (2022).
44. Lercher, L., Danilenko, N., Kirkpatrick, J. & Carlomagno, T. Structural characterization of the Asf1-Rtt109 interaction and its role in histone acetylation. *Nucleic Acids Res* **46**, 2279-2289 (2018).
45. Feng, S. et al. RIF1-ASF1-mediated high-order chromatin structure safeguards genome integrity. *Nat Commun* **13**, 957 (2022).
46. Olijnik, A.-A. et al. Genetic and functional insights into CDA-I prevalence and pathogenesis. *Journal of Medical Genetics* **58**, 185 (2021).
47. Popova, E.Y. et al. Chromatin condensation in terminally differentiating mouse erythroblasts does not involve special architectural proteins but depends on histone deacetylation. *Chromosome Res* **17**, 47-64 (2009).
48. Ji, P., Yeh, V., Ramirez, T., Murata-Hori, M. & Lodish, H.F. Histone deacetylase 2 is required for chromatin condensation and subsequent enucleation of cultured mouse fetal erythroblasts. *Haematologica* **95**, 2013-21 (2010).
49. Hattangadi, S.M. et al. Histones to the cytosol: exportin 7 is essential for normal terminal erythroid nuclear maturation. *Blood* **124**, 1931-40 (2014).
50. Zhao, B. et al. Nuclear Condensation during Mouse Erythropoiesis Requires Caspase-3-Mediated Nuclear Opening. *Dev Cell* **36**, 498-510 (2016).
51. Roy, N.B.A. & Babbs, C. The pathogenesis, diagnosis and management of congenital dyserythropoietic anaemia type I. *Br J Haematol* **185**, 436-449 (2019).
52. Marra, R. et al. Unveiling the genetic landscape of suspected congenital dyserythropoietic anemia type I: A retrospective cohort study of 36 patients. *Am J Hematol* (2024).
53. Kastner, B. et al. GraFix: sample preparation for single-particle electron cryomicroscopy. *Nature Methods* **5**, 53-55 (2008).
54. Punjani, A., Rubinstein, J.L., Fleet, D.J. & Brubaker, M.A. cryoSPARC: algorithms for rapid unsupervised cryo-EM structure determination. *Nature Methods* **14**, 290-296 (2017).
55. Zheng, S.Q., Palovcak, E., Armache, J.-P., Cheng, Y. & Agard, D.A. Anisotropic Correction of Beam-induced Motion for Improved Single-particle Electron Cryo-microscopy. *bioRxiv*, 061960 (2016).
56. Rohou, A. & Grigorieff, N. CTFFIND4: Fast and accurate defocus estimation from electron micrographs. *Journal of Structural Biology* **192**, 216-221 (2015).
57. Bepler, T. et al. Positive-unlabeled convolutional neural networks for particle picking in cryo-electron micrographs. *Nature Methods* **16**, 1153-1160 (2019).
58. Rubinstein, J.L. & Brubaker, M.A. Alignment of cryo-EM movies of individual particles by optimization of image translations. *Journal of Structural Biology* **192**, 188-195 (2015).
59. Zivanov, J., Nakane, T. & Scheres, S.H.W. Estimation of high-order aberrations and anisotropic magnification from cryo-EM data sets in RELION-3.1. *IUCrJ* **7**, 253-267 (2020).
60. Punjani, A., Zhang, H. & Fleet, D.J. Non-uniform refinement: adaptive regularization improves single-particle cryo-EM reconstruction. *Nature Methods* **17**, 1214-1221 (2020).
61. Pettersen, E.F. et al. UCSF ChimeraX: Structure visualization for researchers, educators, and developers. *Protein Sci* **30**, 70-82 (2021).
62. Emsley, P., Lohkamp, B., Scott, W.G. & Cowtan, K. Features and development of Coot. *Acta Crystallogr D Biol Crystallogr* **66**, 486-501 (2010).
63. Liebschner, D. et al. Macromolecular structure determination using X-rays, neutrons and electrons: recent developments in Phenix. *Acta Crystallographica Section D* **75**, 861-877 (2019).

64. Croll, T. ISOLDE: a physically realistic environment for model building into low-resolution electron-density maps. *Acta Crystallographica Section D* **74**, 519-530 (2018).
65. Mazo, G. QuickFigures: A toolkit and ImageJ PlugIn to quickly transform microscope images into scientific figures. *PLoS One* **16**, e0240280 (2021).

Table 1. Cryo-EM data collection and processing statistics.

CODANIN-1 and ASF1A complex (EMD-60697, PDB 9IMZ)	
Data collection and processing	
Camera	K3
Magnification (nominal)	x81,000
Voltage (kV)	300
Number of micrographs	4,282
Electron exposure (e-/Å^2)	58.9
Number of frames collected	50
Energy filter slit width (eV)	18
Defocus range (μm)	-0.8 to -2.4
Pixel size (Å)	1.1
Symmetry imposed	C2
Initial particle images (no.)	1,592,795
Final particle images (no.)	221,978
Map resolution (Å) (masked)	3.56
FSC threshold	0.143
Map sharpening B factor (Å^2)	-50.34
Refinement	
Final EM map	EMD-60697
Atomic model	PDB 9IMZ
Initial model used (PDB code)	PDB 2IO5 for ASF1A
Refinement package	Phenix
Model-map scores	
Model-map correlation Coefficients CC (masked)	0.82
Model composition	
Non-hydrogen atoms	10,696
Protein residues	1,336
R.m.s. deviations	
Bond lengths (Å)	0.007
Bond angles (º)	1.002
C-beta outliers (%)	0
Validation	
MolProbity score	0.78
Clashscore	0.84
Poor rotamers (%)	0
Ramachandran plot	
Favored (%)	97.92
Allowed (%)	2.08
Disallowed (%)	0